Scripta METALLURGICA et MATERIALIA
Vol. 25, pp. 1901-1906, 1991
Printed in the U.S.A.

CREEP DEFORMATION AND FRACTURE OF A TWO-PHASE TiAl ALLOY

J. S. Huang
Chemistry and Materials Science Department
Lawrence Livermore National Laboratory
P.O. Box 808, L-352, Livermore, CA 94550

Young-Won Kim
Metcut-Materials Research Group
P.O. Box 33511
Wright-Patterson AFB, OH 45433-0511

(Received April 29, 1991)
(Revised June 3, 1991)

Introduction

Gamma TiAl ($L1_0$ structure), which is structurally stable up to about 1460 °C and exhibits good specific strength, modulus, and oxidation resistance at high temperature, is a potential candidate structural material for high temperature service such as required for heat engines. Due to its inherent brittleness at ambient temperature, extensive efforts have been made in recent years to develop more ductile alloys. This was primarily done through additions of Cr, V, Mn, Nb, and Ta, and manipulation of microstructure for two-phase (gamma+alpha-2) alloys based on Ti-(47-49)at.%Al (1, 2). Depending upon heat treatments, these alloys exhibit four different types of microstructure: fully-lamellar, nearly-lamellar, duplex, and nearly-gamma (2, 3). Fully-lamellar structures consisting of large grains with alternating gamma and alpha-2 platelets are known to yield high toughness and creep resistance, and duplex microstructures result in the highest ductility at room temperature (2, 4). A number of researchers have studied the deformation behavior of single-phase TiAl alloys (5-8), while there are only limited number of reports on the deformation behavior of two-phase alloys (9, 10). The results show that in single phase(gamma) Ti-(52-54)at.%Al binaries, the slip systems are{111} planes and dislocations of a/2<110>, a<101> and a/2 <112> types are present. The a<101> and a/2<112> dislocations are superdislocations, which were found to undergo complex dissociation reactions, creating sessile faulted dipoles and contributing to the brittleness of TiAl alloys (5, 8). For two-phase alloys, only the easy-slip type unit dislocation a/2<110> and {111} twins were present after tensile deformation at room temperature. The deformation mechanism of TiAl alloys at high temperature under creeping condition is not sufficiently studied. Loiseau and Lasalmonie (7) studied single-phase alloys with Al between 50 and 56 at.%, and observed twinning deformation up to 800 °C. As the temperature increases, the tendency for deformation by twinning is decreased. Both a<101> superdislocations and a/2<110> unit dislocations have been observed.

Although TiAl alloys have good oxidation resistance, it has been reported that inward diffusion of oxygen causes embrittlement of the alloys. This presents a problem when the material is undergoing creep in an oxygen environment. The embrittlement could facilitate crack initiation and growth (creep crack growth) from the surface and shorten the creep rupture life of the material at high temperature. To better understand the effect of oxidation on deformation and fracture at high temperature, we studied the creep behavior of a two-phase alloy in vacuum and in air.

Experimental

The two-phase ($\gamma+\alpha_2$) alloy has the following nominal composition: Ti-47.0Al-1.0Cr-1.0V-2.5Nb(at.%). The interstitial contents were determined to be: O: 580 wt.ppm, N: 55 wt.ppm; C: 160 wt.ppm; and H: 14 wt.ppm. The alloy was prepared by skull melting and casting, followed by hot isostatic pressing at 1200 °C for four hours, and then by extrusion at 1290 °C with an extrusion ratio of 6:1. The extruded bars were annealed at 1360 °C for four hours followed by air cooling and then aged at 1000 °C for 6 hours. The heat treatment was

0036-9748/91 $3.00 + .00

intended to form a fully-lamellar microstructure. A preliminary study indicated that this heat treatment result in a yield strength of 518 MPa at room temperature and 316 MPa at 900 °C. The heat treated bars were machined into tensile specimens with the gage section having a diameter of 2.54 mm and length of 19 mm. Creep tests were conducted in vacuum and in air at 900 °C. The vacuum was 4 x 10^{-6} Pa during testing. Three nominal stress levels, 138, 207 and 276 MPa, were studied in vacuum, and two nominal stress levels, 138 and 207 MPa, were studied in air. For tests in vacuum, the elongation of the gauge section was monitored using an optical travelling telescope. For tests in air, oxidation of the samples made the strain monitoring more difficult and only the time to creep rupture was measured. Conventional optical microscopy, wavelength dispersive x-ray spectroscopy (WDS), scanning electron (SEM) and transmission electron microscopy (TEM) were used to study the microstructure of the alloy before creep testing. After creep testing, TEM samples were prepared from the longitudinal cross sections of tested specimens to study dislocation structure. TEM was conducted with a JEOL 200-CX electron microscope, and SEM and WDS analyses with a JEOL Superprobe-733 electron microprobe.

Experimental Results and Discussion

Figure 1 shows a backscattered-electron SEM image of the microstructure of the alloy, exhibiting an almost fully-lamellar structure containing fine gamma grains along the grain boundaries of large lamellar grains. TEM analysis indicated that the gamma grains has the $L1_0$ structure of TiAl. A minor phase, which imaged bright along the grain boundaries of these gamma grains, was identified with TEM as the alpha-2 Ti_3Al phase. The large lamellar grains in Fig. 1 consist of intermixing platelets which were confirmed by TEM analysis and WDS x-ray microanalysis to be the $L1_0$ TiAl phase and the alpha-2 Ti_3Al phase. These platelets had a usual crystallographic relationships, $(011)_\gamma // (0001)_{\alpha_2}$ and $<110>_\gamma // <2\bar{1}10>_{\alpha_2}$; however, not all of the neighboring gamma platelets are separated by a Ti_3Al platelet existed between them.

Table 1 summarizes the test parameters and results including time to rupture, diameter of ruptured sample and reduction of area at the location of fracture. The time to rupture *versus* stress is plotted in Fig. 2. The exposure to oxygen during testing significantly reduced the time to rupture of the alloy by a factor of more than 20. As an example, at a stress level of 207 MPa, the time to rupture is 238 hour in vacuum and only 10 hours in air. The exposure to air also reduced the ductility prior to fracture as indicated by the reduction of area. Despite creep deformation being a bulk deformation phenomenon, creep fracture of this alloy is strongly sensitive to oxidation, which is a surface phenomenon. As shown later, this could be attributed to the fact that the creep failure of this alloy occurs primarily by creep crack growth.

The creep behavior (strain *versus* time) for the samples tested in vacuum is shown in Fig. 3a. It is typical of the three-stage behavior observed in metals and alloys. It is noted that the duration of the steady-state creep-rate regime is relatively short compared to the duration of the third-stage creep, except for the test at 159 MPa which was stopped before it reached the third-stage creep. This behavior of long third-stage creep can probably be attributed to the early on-set of grain boundary creep crack initiation and growth. The steady-state creep rate is plotted *versus* stress in Fig. 3b. The stress sensitivity exponent for creep rate is calculated as 5.8. Values ranging from 4.5 to 5.7 have been reported for both single-phase and two phase TiAl alloys. (11-13)

Table 1. Results of creep testing of the two-phase Ti-47Al-1Cr-1V-2.5Nb alloy at 900 °C in air and in vacuum (Df: the diameter of sample at the location of fracture.)

Sample No.	Stress (MPa)	Time to rupture (hour)	Df (mm)	Reduction of area (%)
G171-2 (vacuum)	276	49	2.03	36
G171-1 (vacuum)	207	238	2.01	38
G171-3 (vacuum)	159	>225*	N/A	N/A
G171-4 (air)	207	10	2.26	21
G171-5 (air)	159	24	2.39	12

* test stopped.

Figure 4 shows a longitudinal cross-sectional optical micrograph of the sample tested in vacuum at 207 MPa. The fracture is mainly intergranular, although transgranular fracture is also present. The transgranular fracture is probably developed by overloading during the last stage of the creep testing. Figure 5 shows a photograph of the surface of this sample which indicates that a large grain boundary void or crack has developed at a location away from the fracture surface. This further indicates the the creep fracture of this alloy is primarily caused by intergranular crack initiation and growth. SEM fractographs of the fracture surface of this same sample are shown in Fig. 6 at different magnifications. The fracture is typical of that caused by cavity nucleation, growth and coalescence. The mode of fracture in air is shown in Fig. 7, the longitudinal cross-sectional optical micrograph of the sample tested at 207 MPa. As in vacuum, the fracture is primarily intergranular and some secondary cracks develop along interlamellae interfaces in the final stage of fracture. Exposure to air during and after testing caused oxide scales to form on the surfaces of these cracks. There is very little necking for the sample, indicating that creep fracture of this alloy occurred primarily with initiation and growth of cracks from the surface (creep crack growth). The fact that creep rupture life in air is much lower than that in vacuum suggests that oxidation assists initiation and growth of grain boundary cracks.

Figure 8 shows a low magnification TEM bright field image of the sample tested in vacuum at a stress 207 MPa. Dislocations exist in both gamma grains and lamellar grains. A dislocation cell structure is also developed in grain boundary gamma grains possibly due to dynamic recrystallization. Figure 9 shows four images of dislocations in one of the lamellar grains taken with four different reciprocal lattice vectors (g). Using the $g.b = 0$ criteria for the invisibility of dislocation, it was shown that the dislocations in both gamma grains and lamellar grains are of the a/2<110] type. We did not observe superdislocations nor any evidence of twin deformation. Our study further indicated that deformation took place in almost all cases in the gamma phase only and the alpha-2 plates were almost intact. The slow creep rates measured in this experiment may be due to the large grain size as well as the laminated composite nature of the lamellar grains. Similar results were obtained for the samples tested in air. Previous studies have shown that in two-phase alloys with Al less than 49 at.%, superdislocations do not exist after tensile deformation. The current results indicate this is also true in creep-deformed samples. Since the strain rate is much smaller in creep testing than in tensile testing, one may conclude that there is no significant effect of strain rate on the nature of operative dislocations.

The most significant result in this work is that the creep fracture of this alloy is very sensitive to oxidation. This is in contrast to the result (6) that after prior oxidation, tensile properties of TiAl alloys are not affected. This difference is understandable since creep testing is a long term test which allows oxygen to diffuse toward the crack tip. From the alloy development view-point, evaluation of creep rupture in vacuum and in air may be a preferred way to study oxidation resistance when the material is under stress.

Acknowledgments

We wish to thank Mr. G. F. Gallegos and Dr. D.Dimiduk for interesting discussions and support of this work. We also thank Mr. M. Wall for his assistance in transmission electron microscopy. This work was performed under the auspices of the U.S. Department of Energy by the Lawrence Livermore National laboratory under contract W-7405-Eng-48, and the U.S. Air Force Wright Patterson Laboratory, Materials Directorate under contract F33615-89-C-5629.

References

1. Y-W. Kim, JOM, 41, 7, 24-30 (1989).
2. Y-W. Kim, *Mat. Res. Soc. Symp. Proc.* 213, (1991), in print.
3. Y-W. Kim, Act. Met. (1991), submitted for publication.
4. D. S. Shih and S-C. Huang, *Microstructure/Property Relationships in Titanium Aluminides and Alloys*, ed. Y-W. Kim and R. R. Boyer, TMS, Warrendale, PA (1990), in print.
5. D. Shechtman, M. J. Blackburn, and H. A. Lipsitt, Met. Trans. A, 5, 1373-1381 (1974).
6. H. A.Lipsitt, Dan Shechtman,and R. E. Schafrik, Met. Trans. A, 6, 1991-1996 (1975).
7. A. Loiseau and A. Lasalmonie, Mater. Sci. and Eng., 67, 163-168 (1984).
8. G. Hug, A. Loiseau, and A. Lasalmonie, Phil. Mag. A, 54, 47-65 (1986).
9. E. L. Hall and S. C. Huang, J. Mater. Res., 4, 595-602 (1989).
10. V. K Vasudevan, M. A. Stucke, S. A. Court, and H. L. Fraser, Phil. Mag. Letters, 59, 299-307 (1989).
11. T. Takahashi and H. Oikawa, *Mat. Res. Soc. Symp. Proc.* 133, 699 (1989), Materials Research Society, Pittsburgh, PA.
12. H. Oikawa, *High Temperature Aluminides and Intermetallics*, ed. S. H. Whang, C. T. Liu, D. P. Pope, and J. O. Stiegler, 353 (1990), TMS, Warrendale, PA.
13. P. L. Martin, M. G. Mendiratta, and H. A. Lipsitt, Met. Trans. A, 14, 2170-2174 (1983).

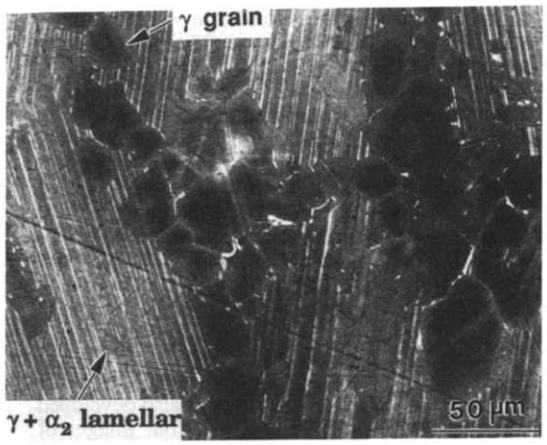

FIG. 1. SEM back-scatter-electron image of the microstructure of the two-phase TiAl alloy.

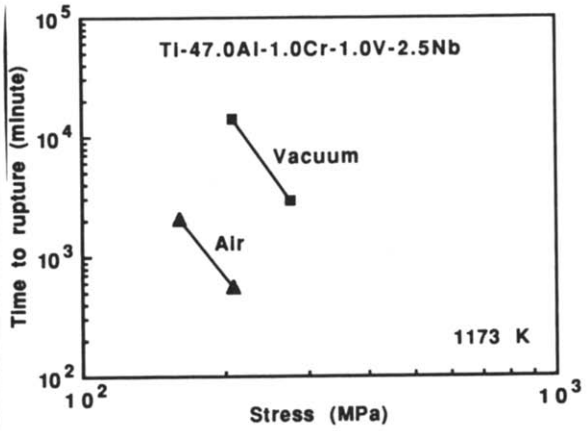

FIG. 2. Time to rupture *vs* stress for the two-phase TiAl alloy creep-tested in air and in vacuum and at 1173 K.

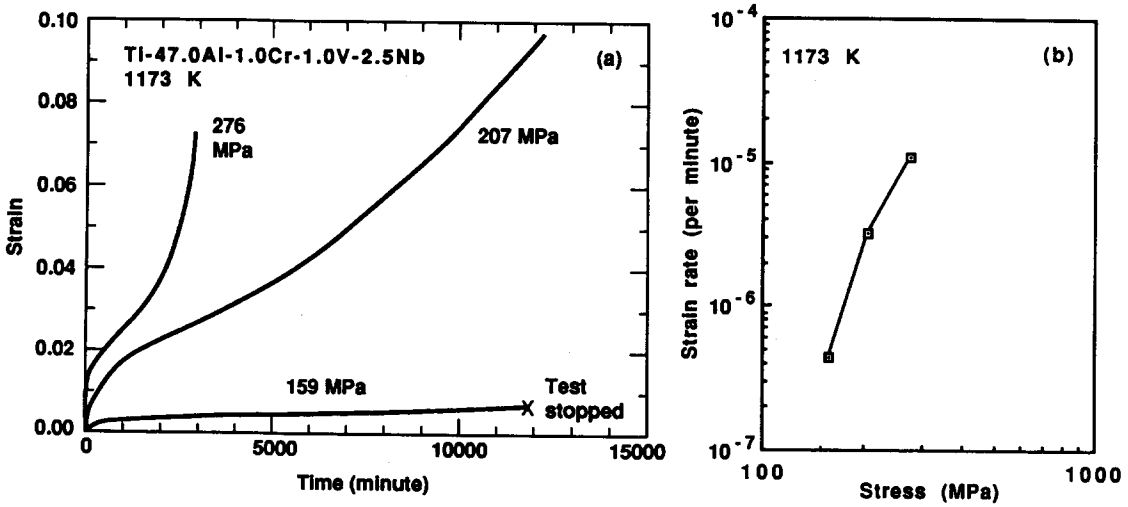

FIG. 3. Creep behavior of the two-phase TiAl alloy at 1173 K in vacuum. (a) Creep strain *versus* time; (b) Steady-state creep rate *versus* stress.

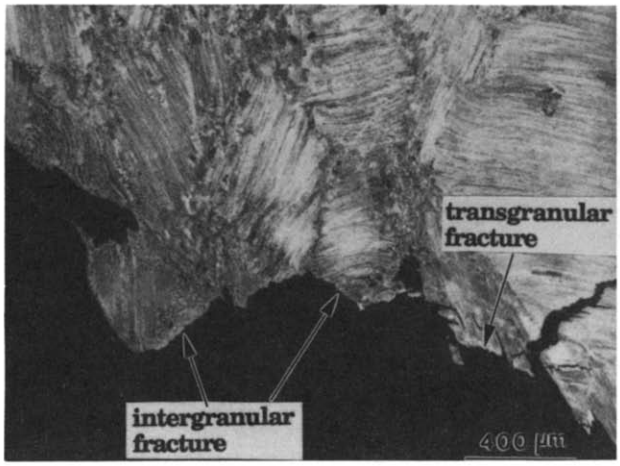

FIG. 4. Optical micrograph of a longitudinal cross section of the sample tested in vacuum at 207 MPa, showing both intergranular and transgranular fractures and secondary cracking.

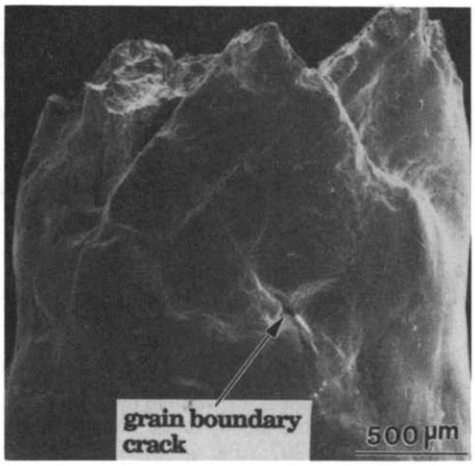

FIG. 5. Photograph of the sample tested in vacuum at 207 MPa showing the grain boundary crack initiated from the surface.

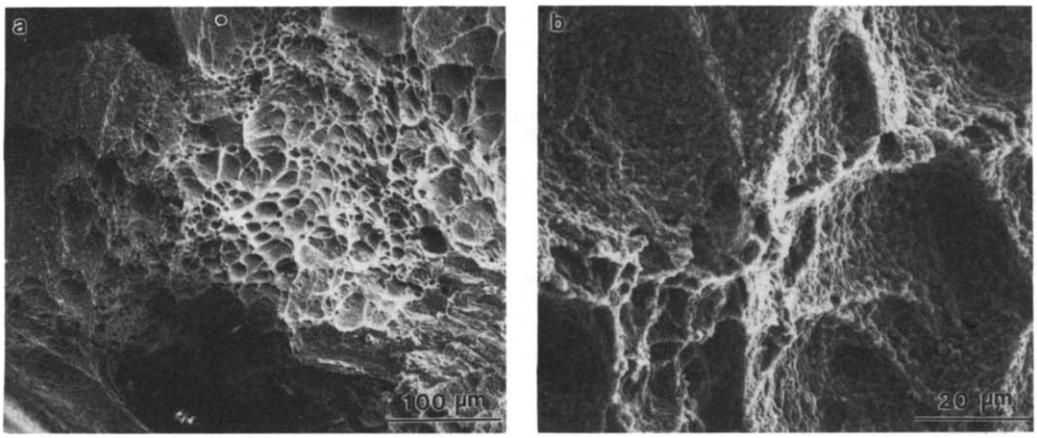

FIG. 6. SEM micrographs of the fracture surface of the sample tested in vacuum and at 207 MPa, at low (a) and high (b) magnifications, showing dimple fracture.

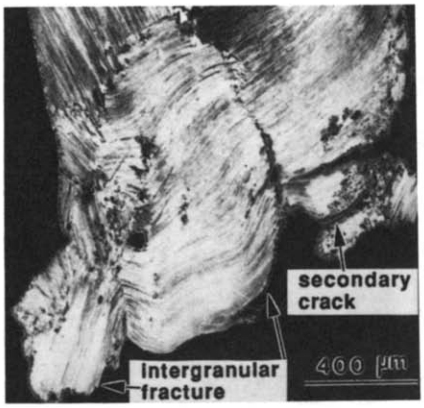

FIG. 7. Optical micrograph of longitudinal cross section of the sample tested in air at 207 MPa.

FIG. 8. TEM image of the general dislocation structure of the sample tested in vacuum at 207 MPa.

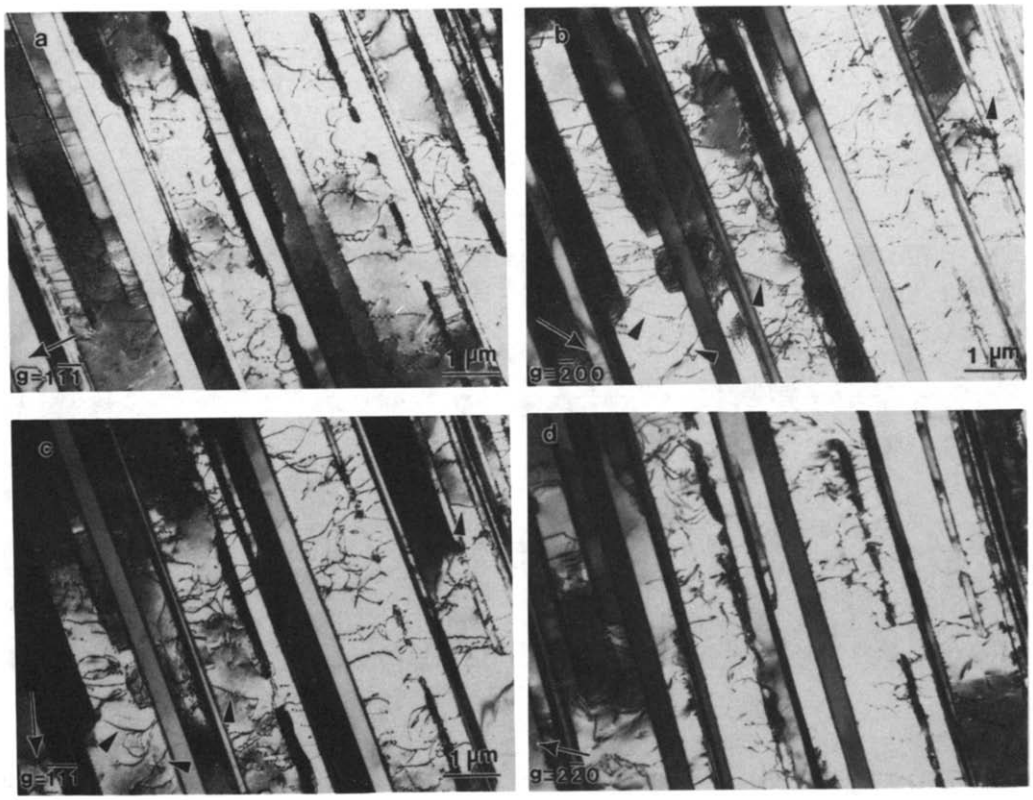

FIG. 9. TEM images of dislocations in the lamellar structure near the fracture surface of sample tested in vacuum at 207 MPa, taken with four different reciprocal lattice vectors, g. The lamellar structure consists of twin-related gamma with very thin (<0.1 μm) alpha-2 platelets. Note that the dislocations pointed by triangle markers are visible in (c) and (b), but invisible in (a) and (d).